frontiers | Frontiers in Materials

ORIGINAL RESEARCH
published: 27 June 2022
doi: 10.3389/fmats.2022.934215

High Temperature Oxidation Behavior of Nano-Alumina–Modified NiAl Coating

Yuqing Fang[1,2], *Xiaoyong Shu*[1,2]* *and Shuhe Dong*[1,2]

[1]School of Materials Science and Engineering, Nanchang Hangkong University, Nanchang, China, [2]Jiangxi Aviation Material Surface Technology Engineering Center, Nanchang, China

In this article, the nickel aluminide coating prepared by the chemical vapor deposition method has adhered deliberately with nano-alumina film on the surface by the electrophoresis method. The analysis results of oxidation behavior in the air at 1,000°C reported that the nano-alumina particles adhering to the nickel aluminide coating surface appear to be effective in facilitating the θ-Al_2O_3 to α-Al_2O_3 phase transformation. The fast θ to α phase transformation helps reduce the oxidation rate of the nickel–aluminum coating and prevents the cracking and peeling in the oxide scale. The research addressed a novel method to improve the high-temperature oxidation resistance of nickel aluminide coatings.

Keywords: Nickel aluminide coating, alumina modified, high temperature, oxidation, phase transition

OPEN ACCESS

Edited by:
Yi Xu,
Nanchang University, China

Reviewed by:
Zenghua Gao,
Aerospace Special Materials and Processing Technology Institute
Beijing, China
Bo Li,
East China University of Science and Technology, China

***Correspondence:**
Xiaoyong Shu
xiaoyong202@126.com

Specialty section:
This article was submitted to Environmental Degradation of Materials, a section of the journal Frontiers in Materials

Received: *02 May 2022*
Accepted: *16 May 2022*
Published: *27 June 2022*

Citation:
Fang Y, Shu X and Dong S (2022) High Temperature Oxidation Behavior of Nano-Alumina–Modified NiAl Coating. Front. Mater. 9:934215. doi: 10.3389/fmats.2022.934215

INTRODUCTION

Nickel aluminide coatings, such as NiAl and Ni_2Al_3, are generally applied to the surfaces of engine turbine components to lengthen their service life (Goward, 1970; Goward and Boone, 1971; Leng et al., 2020). The common preparation methods of nickel aluminide coatings include slurry, powder embedding, physical vapor deposition, and chemical vapor deposition (CVD) (Nicholls, 2003; Bouchaud et al., 2013; Mollard et al., 2013; Montero et al., 2013). Compared with the other methods, the coating prepared by the CVD method has a stronger bonding force with the substrate and is denser, so its high-temperature oxidation resistance is better (Warnes and Punola, 1997; Yavorska et al., 2011; Goral et al., 2020).

The surface of the nickel aluminide coating will form protective thermally grown oxide (TGO)-Al_2O_3 at high temperatures (Swadba et al., 2011). Several types of Al_2O_3 have been found on alloys forming aluminides, such as γ-Al_2O_3, δ-Al_2O_3, θ-Al_2O_3, and α-Al_2O_3. α-Al_2O_3 is a good protective oxide scale because of its thermodynamic stability and slow growth rate (An et al., 2000). During the oxidation at a temperature above 1,100°C, the nickel aluminide coating quickly forms the thermodynamically stable α-Al_2O_3 scale, while the metastable alumina variants scales (normally γ and θ) are formed after a oxidation for a long time (Khana et al., 2019) at a temperature below 1,100°C, during which they always experience the phase transformation of metastable-to-stable alumina (Peng et al., 2003; Huang and Peng, 2016), such as θ-to-α. This phase transformation accompanies a volume shrinkage of about 10%, sometimes resulting in the generation of micro-cracks in the alumina scale (Peng et al., 2003; Veal et al., 2006; Wang and Zhou, 2012; Huang and Peng, 2016).

As a result, prompting the conversion of metastable-to-stable alumina is advantageous for improving the oxidation resistance of nickel aluminide coatings at high temperatures (Khana et al., 2019). Moreover there is a well-known fact that a rising temperature causes a faster phase transformation of the metastable-to-stable alumina, dopants or template effects have been found

to change this process (Tolpygo and Clarke, 2000; Huang et al., 2019). For instance, Pint and his co-workers (Pint et al., 1997; Huang et al., 2019) found that Y_2O_3, La_2O_3, ZrO_2, and HfO_2 dispersions in β-NiAl tend to retard the θ-to-α phase transformation, whereas TiO_2 dispersion appears to promote this process. Lately, Peng and his co-workers (Xu et al., 2010; Huang and Peng, 2016; Wang et al., 2016; Khana et al., 2019) reported the promoted formation of an α-Al_2O_3 scale on nickel aluminide with surface Cr_2O_3 particles. On these bases, we have a concept that spreading oxide particles (e.g., Cr_2O_3) with the same crystallographic structure as α-Al_2O_3 to aluminide can promote the growth of an α-Al_2O_3 scale at a high temperature (Yin and Zhen, 2015). Valet et al. (Liu et al., 2007; Huang and Peng, 2016; Khana et al., 2019) found that the remaining fine α-Al_2O_3 grits, used for the polishing surface of the intermetallic sample, appeared to promote the nucleation of α-Al_2O_3.

In this article, nano-alumina particles were deposited on the surface of aluminide coatings by electrophoresis, and their effects on the phase transition and oxidation kinetics of the nickel aluminide coatings were investigated. It is aimed to better understand the phase transitions of the oxidative properties of nickel aluminides, and find a more effective way to improve the oxidation resistance of these nickel aluminide oxides by promoting the growth of α-Al_2O_3.

THE EXPERIMENT

The pure nickel samples with dimensions of 10 mm × 10 mm × 2 mm were cut from an electrolyte pure nickel plate. After being abraded to a final 2,000 grit SiC paper, they were ultrasonically cleaned in acetone. By using the CVD method, the Ni_2Al_3 coating was developed on the pure nickel surface after aluminizing at 750°C × 200 torr for 3 h. The preparation process is as follows: high-purity Cl_2 was injected into the reaction chamber containing high-purity aluminum particles (purity: 99.99%, size: 3 mm) to generate gas-phase halide $AlCl_x$. $AlCl_x$ was carried into the deposition chamber by Ar, and then was reduced to activity [Al] by H_2. The [Al] deposited on the pure nickel, and reacted with nickel to form a nickel aluminum coating. After aluminizing for 3 h, the samples were cooled to room temperature with the furnace. The main equations involved in the reaction are as follows:

$$2Al + Cl2_{(g)} \rightarrow 2AlCl_{(g)}, \quad (1)$$

$$Al + Cl2_{(g)} \rightarrow AlCl2_{(g)}, \quad (2)$$

$$2Al + 3Cl2_{(g)} \rightarrow 2AlCl3_{(g)}, \quad (3)$$

$$AlCl_{(g)} + AlCl2_{(g)} + AlCl3_{(g)} + 3H2_{(g)} \rightarrow 3[Al] + 6HCl_{(g)}. \quad (4)$$

The nano-Al_2O_3 film was made to adhere to the nickel aluminum coating surface by electrophoresis technology. High temperature oxidation experiments were performed using the SETSYS evolution thermo-gravimetric analyzer (for *in situ* recording oxidation curves) in the air at 1,000°C for 50 h. A nickel layer was coated on the oxide scale surface using electroplating in the acidic electroless nickel plating mixed solution (containing 25 g/L $C_3H_6O_3$, 6.25 g/L Na_2CO_3, 43 g/L $NiSO_4{\cdot}6H_2O$, and 25 g/L $NaH_2PO_2{\cdot}H_2O$) at 98°C for 5 h. Scanning electron microscope (SEM), energy dispersive spectroscopy (EDS), and X-ray diffraction (XRD) were used to investigate the surface and cross-section morphologies, structure, and the phases of various nickel aluminide coatings.

RESULTS AND DISCUSSION

The cross-sectional morphology (**Figure 1A**) shows that a single layer of nickel aluminide coating (~30 μm thickness) was deposited on pure nickel after aluminizing. The coating was dense and well adherent to the pure Ni substrate. The Ni content and Al content of the coating were 39.3 at.% and 58.9 at.%, respectively. The XRD result (**Figure 1C**) characterized them as deposited coating as a δ-Ni_2Al_3 phase. Backscattered SEM images of the polished cross-section of a nano-Al_2O_3 film sample are shown in **Figure 1B**. The as-electrophoresis Al_2O_3 film was continuous with a thickness of around 3 μm. However, the Al_2O_3 film was partially detached from the coating due to grinding and polishing during the preparation process.

Figure 2 shows the dependence on the time of mass grain and the square of mass grain of naked and Al_2O_3 film-covered Ni_2Al_3 coatings oxidated at 1,000°C for 50 h. The mass grain of Al_2O_3 film-covered Ni_2Al_3 coating is less than that of the naked one as shown in **Figure 2A**. In the early stages of oxidation , the surface of the two types of coatings quickly formed an aluminum oxide scale, and the oxidation weight gain rate was high. Due to the presence of alumina, the contact surface between oxygen and the coating gradually decreased, and the alumina scale gradually stabilized, so the oxidation weight gain curve tended to be flat. As shown in **Figure 2B**, during the 50-h oxidation, the oxidation processes of both coatings can be divided into two stages: In the initial stage (<3 h), the parabolic oxidation rate constant (Kp^I) of the Al_2O_3 film–covered Ni_2Al_3 coating is 3.2×10^{-13} g^2/cm^4s lower than that of the naked coating with parabolic oxidation rate constant Kp^I of ~4.4×10^{-13} g^2/cm^4s. In the steady stage (>3 h), the parabolic oxidation rate constant (Kp^{II}) of the Al_2O_3 film–covered Ni_2Al_3 coating is 1.2×10^{-13} g^2/cm^4s, also lower than that of the naked coating with parabolic oxidation rate constant Kp^{II} of ~2.4×10^{-13} g^2/cm^4 s.

The Al_2O_3 film-covered coating macroscopic surface after oxidation is shown in **Figure 3A**, and then the electrophoretic alumina film was removed using alcohol, as shown in **Figure 3B**. The surface characteristics of the naked Ni_2Al_3 coating changes with the increasing oxidation duration , as illustrated in **Figures 4A,C,E,G**. Fine alumina crystals developed on the surface at the early stage of high-temperature oxidation (30 min), and the color depth difference was caused by the distinct growth directions. The size of thin needle-like alumina crystals grew bigger after 2 h oxidation, and the oxide scale got thicker and denser. After being oxidized for 5 h, some acicular alumina became stagnant, cracks appeared on the surface, and the acicular alumina crystals were rapidly regenerated in the spalling area. After 50 h of oxidation, the oxide scale is mostly composed of acicular alumina and round

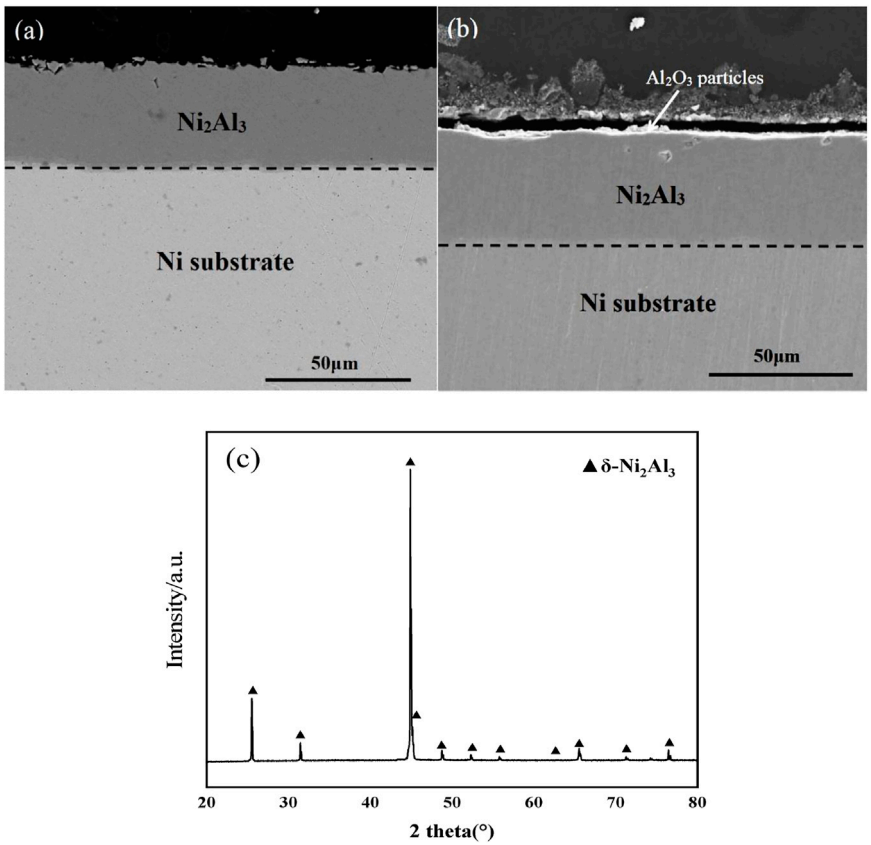

FIGURE 1 | Cross-sectional morphologies of Ni_2Al_3 coatings **(A)** naked, **(B)** with an Al_2O_3 film on the surface, and **(C)** XRD pattern of the naked Ni_2Al_3 coating.

alumina. According to the above morphologies and the characteristics of the alumina phase structure (Swadba et al., 2011), it can be judged that θ-Al_2O_3 is rapidly formed in the early stage of oxidation, and then the θ phase is partially converted into the α phase. The growth of α-Al_2O_3 will inhibit the growth of the θ phase. The lateral growth direction of α-Al_2O_3 resulted in surface unevenness. The conversion of θ phase to α phase will cause the microcracks or even local spalling because of volume shrinkage (the transformation from metastable alumina to α-Al_2O_3 is a reconstructive phase transition, which is a first-order phase transition and the process is irreversible). The spalling area will quickly generate θ-Al_2O_3, so both θ-Al_2O_3 and α-Al_2O_3 phases can be seen on the surface after high-temperature oxidation for 50 h. For the Al_2O_3 film–covered Ni_2Al_3 coating, an α-Al_2O_3 scale was formed rapidly in the early stage of oxidation. With the prolongation of oxidation time, the oxide scale gradually thickens and becomes flat (**Figures 4B,D,F,H**). After 5 h of oxidation, the scale appeared to slightly peel. After 50 h of oxidation, a dense and stable alumina scale has been formed. Therefore, there is no phase change in the oxide scale of the Al_2O_3 film–covered coating during the whole oxidation process. It can be seen in **Figure 5A** that the coating degradation completely conforms to the mechanism of the nickel–aluminum coating: δ-Ni_2Al_3→β-NiAl→γ′-Ni_3Al. At the beginning of oxidation, the generated alumina is too thin and its X-ray diffraction peak intensity is weak, so the original diffraction peak pattern is partially enlarged as shown in **Figures 5B′,C′**, from which it is known that the α phase is formed on the surface of the electrophoretic alumina film sample from the beginning of oxidation. Based on the XRD, SEM, and TGA analysis, the early oxidation progress of aluminide in the absence and presence of the surface Al_2O_3 film is shown in **Figure 6**. At the beginning of oxidation (Stage Ⅰ), θ-Al_2O_3 is rapidly formed on the naked aluminide surface, while α-Al_2O_3 is formed on the surface of the aluminide coating with electrophoretic Al_2O_3 particles (An et al., 2000). Then both increase to form an alumina scale (Stage Ⅱ); the alumina is much denser as shown in **Figures 4C,D**. In stage Ⅲ, generated α-Al_2O_3 grows inward and outward at the same time, during which the most electrophoresed Al_2O_3 film on the surface is pushed outward, and a small part is wrapped by the outwardly growing α-Al_2O_3 (Huang and Peng, 2016). At this time, the exposed θ-Al_2O_3 of the naked sample transforms into α-Al_2O_3 (**Figure 4E**). With α-Al_2O_3 gradually increasing, an α-Al_2O_3 scale was formed at the interface between NiAl coating and θ-Al_2O_3 (Stage Ⅳ). During this phase transition, volume shrinkage will occur, resulting in cracks or even peeling of the scale (Tolpygo and Clarke, 2000), which are visible on the surface topography (**Figure 4**).

The nickel aluminide thermally grows θ-Al_2O_3 before α-Al_2O_3 because the former has lower surface energies and thus a much

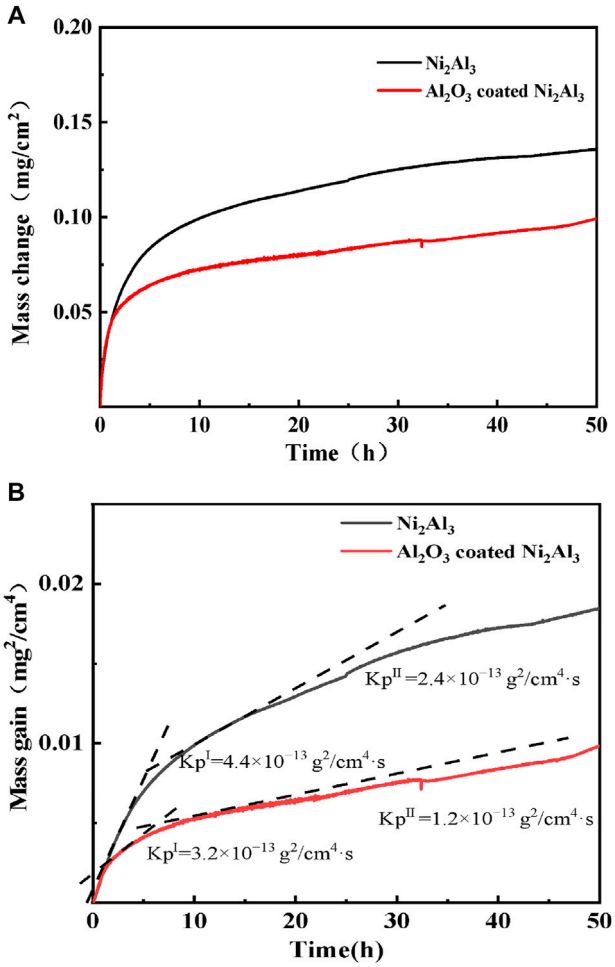

FIGURE 2 | (A) Oxidation kinetics curves and **(B)** corresponding parabolic plots of naked and Al_2O_3 film–covered Ni_2Al_3 coatings oxidated in air at 1,000 °C.

lower nucleation barrier ΔG*. This is the direct origin of why the metastable alumina phases rather than the most stable ones usually form during the initial oxidation of β-NiAl (Huang et al., 2019). Therefore, during the subsequent oxidation, the undesirable metastable-to-stable phase transformation of alumina becomes unavoidable. The direct α-Al_2O_3 formation without metastable-to-stable alumina phase transformation on typical oxide particles (e.g., α-Al_2O_3, Cr_2O_3, and Fe_2O_3) means that the template effect of the oxides isostructural to α-Al_2O_3 intrinsically reduces ΔG* of α-Al_2O_3 down to such a level in favor of its thermal nucleation (Pint et al., 1997; Wang and Zhou, 2012; Yin and Zhen, 2015; Huang et al., 2019). The template effect has been widely studied by revealing some oxides (e.g., Cr_2O_3 and Fe_2O_3), which are isostructural to α-Al_2O_3, and may serve as the nucleation sites facilitating the growth of the α-Al_2O_3 (Pint et al., 1997; Wang and Zhou, 2012; Yin and Zhen, 2015; Huang et al., 2019). This interpretation coincides well with a promoted θ-to-α alumina phase transformation on β-NiAl when it has been embedded with the fine particles of α-Al_2O_3 (Veal et al., 2006). The electrophoretic α-Al_2O_3 particles have the same HCP crystal structure as the α-Al_2O_3 grown from the coating and can act as an epitaxial growth platform for α-Al_2O_3 during oxidation, reducing the nucleation energy of the latter. Therefore, when the surface is completely covered with alumina nanoparticles, the θ-to-α phase transition can be skipped when the coating is oxidized at 1,000°C, and α-Al_2O_3 is directly generated.

The Al_2O_3 particle pretreatment significantly decreases the oxidation rate, leading to a slower degradation rate of the nickel aluminide. As seen in the cross-sectional characteristics in **Figure 7**, after 50 h of oxidation, the phase structures of both types of coatings are NiAl + Ni_3Al phases, indicating that the unstable δ-Ni_2Al_3 phase degenerates into the NiAl phase at a high temperature of 1,000 °C, and then unceasingly degenerates into the Ni_3Al phase with oxidation time prolongation. In **Figure 7**, the thickness of the naked coating and the Al_2O_3 film–covered

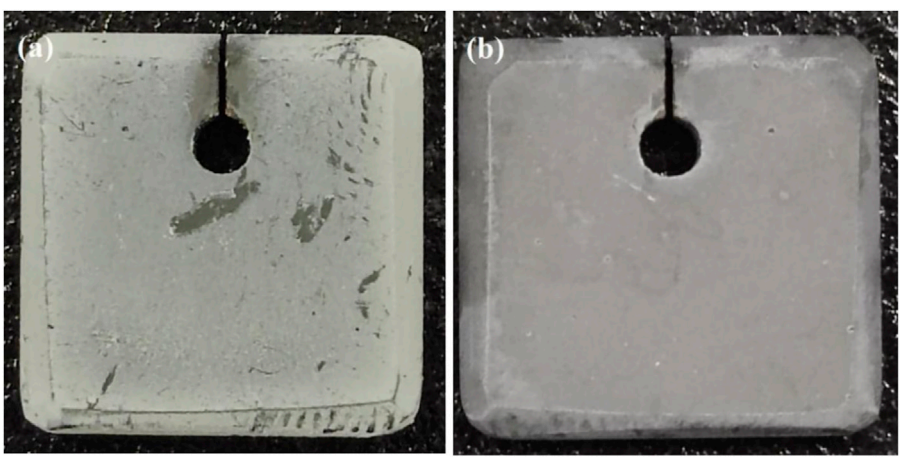

FIGURE 3 | Surface with **(A)** alumina particles after oxidation and **(B)** removal of alumina particles after oxidation.

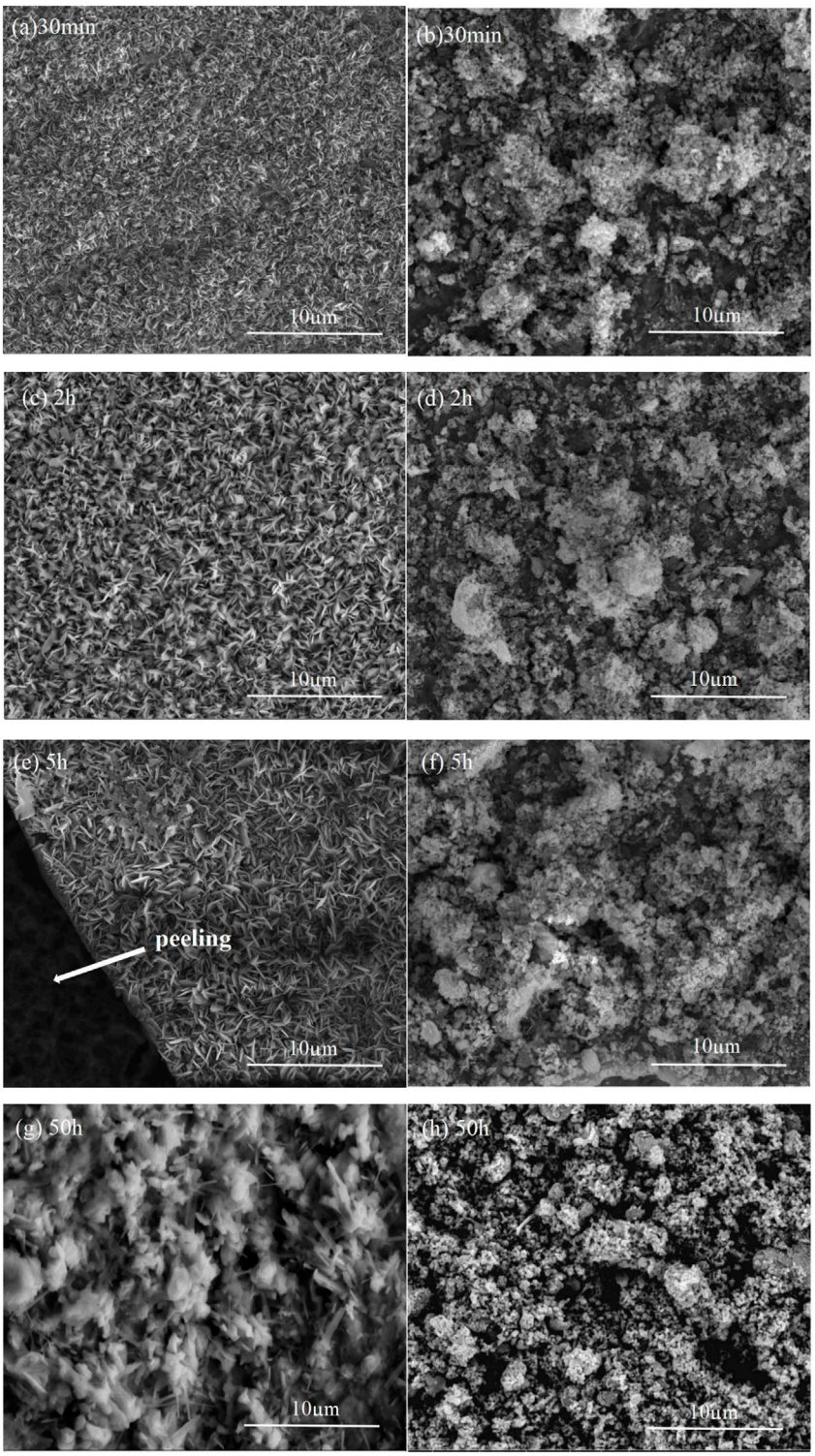

FIGURE 4 | Surface morphologies of the alumina scale formed on the δ-Ni_2Al_3 coating at 1,000°C for different oxidation times. **(A)**, **(C)**, **(E)**, and **(G)**: Ni_2Al_3; **(B)**, **(D)**, **(F)**, and **(H)**: Al_2O_3 film–covered Ni_2Al_3.

coating after oxidation is thicker than that before oxidation, indicating that both coatings have a certain degree of Al elements internal-diffusion during the high-temperature oxidation process. It can be seen from **Figures 7A,B** that the alumina scale thickness of the naked coating is about 7.9 μm, which is twice that of the Al_2O_3-scale–covered coating (~3.5 μm).

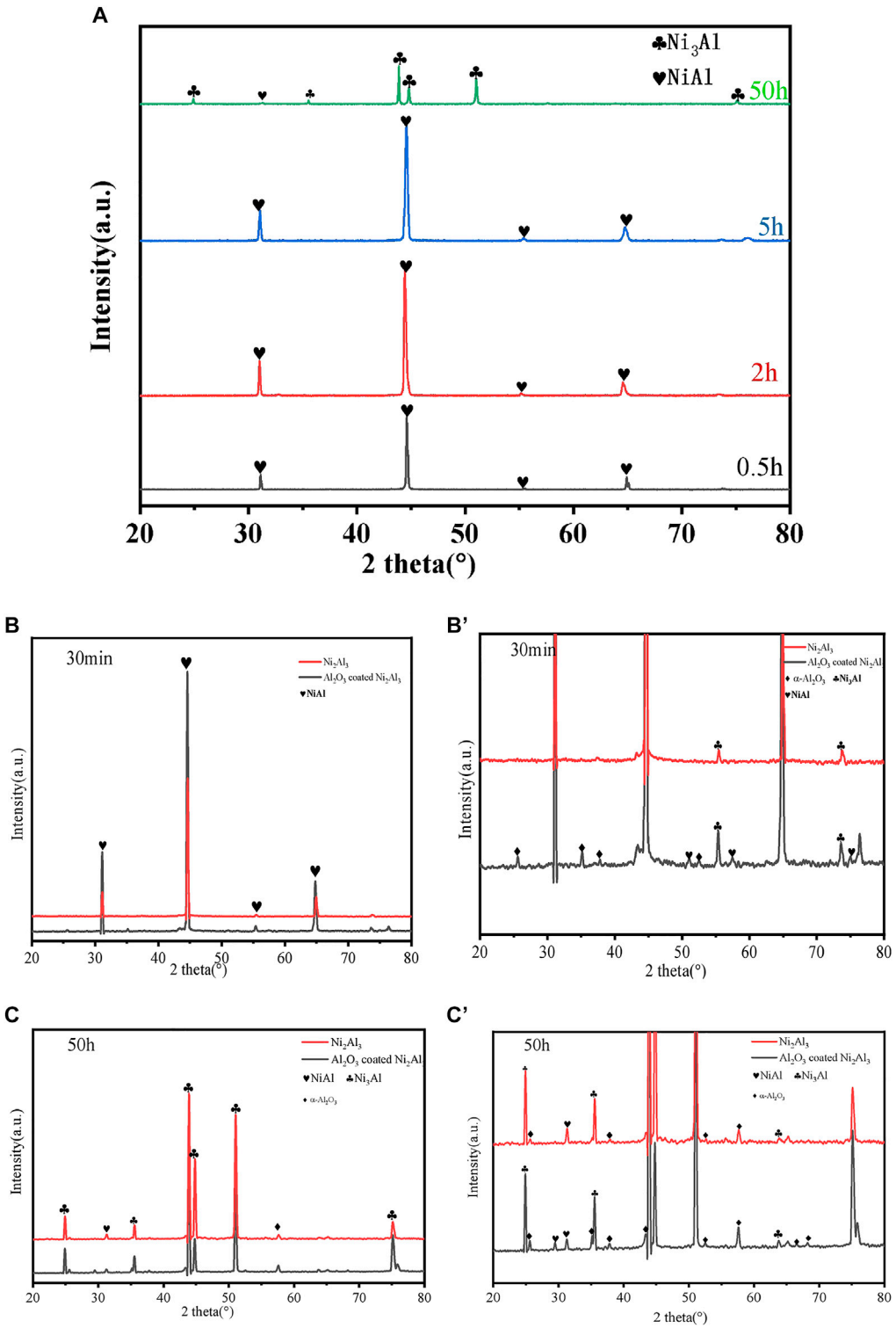

FIGURE 5 | XRD patterns of **(A)** Ni_2Al_3 coating at different times and **(B)** and **(C)** 30 min and 50 h naked and the Al_2O_3 film–covered Ni_2Al_3 coating after oxidation in the air at 1,000°C and **(B′) (C′)** locally magnified.

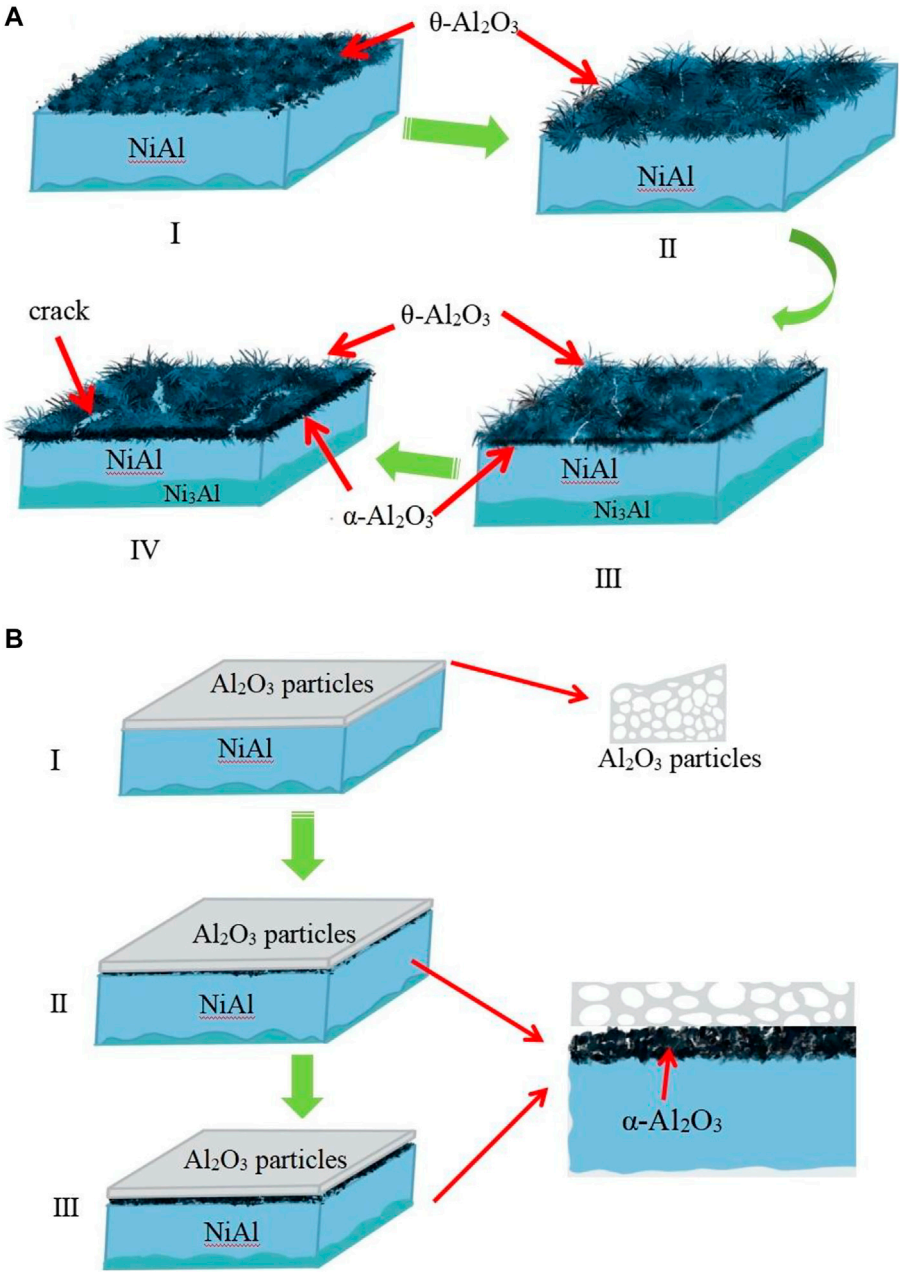

FIGURE 6 | Schematic transient oxidation progress of the Ni_2Al_3 coatings **(A)** without and **(B)** with the surface Al_2O_3 particles.

This is consistent with the analysis result of the oxidation growth curve. During the oxidation process, aluminum ions moving from the inside of the coating to the coating surface meet with oxygen atoms to form an aluminum oxide scale, so there will be a γ-Ni_3Al phase formed due to the Al rapid consumption between the aluminum oxide film and the nickel–aluminum coating. Since the naked coating needs to consume more Al elements to form the aluminum oxide scale, the thickness of the γ-Ni_3Al phase coating is significantly thicker than that of the Al_2O_3 film–covered coating, which is near the aluminum oxide scale. The reason for the difference in the thickness of the two coatings is that electrophoretic alumina can promote the formation of α-Al_2O_3 on the coating surface, which can effectively prevent the oxygen element from entering the coating, reducing the consumption of the Ni_2Al_3 coating. Therefore, promoting the formation of stable-phase α-Al_2O_3 is an effective way to improve the high-temperature oxidation resistance and prolong the life of the coating. The large difference in coating consumption in the same sample is due to the consumption of aluminum elements again to form an aluminum oxide scale after the local scale peels off. With the prolongation of oxidation time, the cracks increase and cause local peeling of the aluminum oxide scale. The spalled

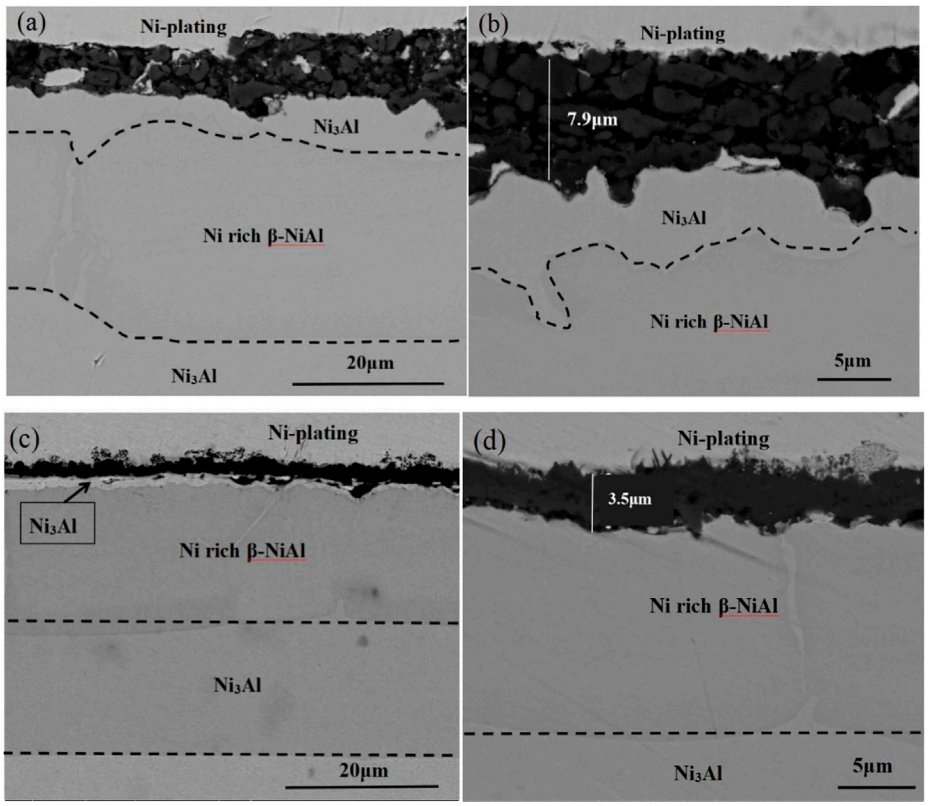

FIGURE 7 | Cross-sectional morphologies of the Al_2O_3 scales on the **(A)** and **(B)** naked Ni_2Al_3 coating, and **(C)** and **(D)** the Al_2O_3 film–covered Ni_2Al_3 after 50 h of oxidation in the air at 1,000°C.

area will quickly deplete the nickel–aluminum coating to form a new aluminum oxide scale.

CONCLUSION

The Ni_2Al_3 coating with a thickness of 35 μm was prepared on the pure Ni matrix using a chemical vapor deposition method at 750°C × 200 T for 3 h, and then the Al_2O_3 film was made to adhere to the Ni_2Al_3 coating surface by electrophoresis technology. Because of the lower power required to form the critical nuclei, the θ-Al_2O_3 formed earlier on the naked Ni_2Al_3 coating and then undergo a θ-to-α Al_2O_3 transition process during the oxidation process at 1,000 °C. The electrophoretic Al_2O_3 film adhering to Ni_2Al_3 coating can skip this phase transition because the Al_2O_3 film on the coating surface can provide a crystal template to promote the nucleation of α-Al_2O_3 at the beginning of oxidation. The rapid nucleation of α-Al_2O_3 significantly reduces the oxidation rate of NiAl coating and prevents microcracks and voids caused by phase transformation.

DATA AVAILABILITY STATEMENT

The original contributions presented in the study are included in the article/supplementary material; further inquiries can be directed to the corresponding author.

AUTHOR CONTRIBUTIONS

YF carried out experiments; XS directed the experiment and analyzed experimental results; SD analyzed experimental results.

FUNDING

The work is supported by the Graduate Innovation Special Fund Project of Nanchang Hangkong University (project Grant No. YC2021-S660).

REFERENCES

An, T. F., Guan, H. R., Sun, X. F., and Hu, Z. Q. (2000). Effect of the θ–α-Al_2O_3 Transformation in Scales on the Oxidation Behavior of a Nickel-Base Superalloy with an Aluminide Diffusion Coating. *Oxid. Mater.* 54, 301–316.

Bouchaud, B., Rannou, B., and Pedraza, F. (2013). Slurry Aluminizing Mechanisms of Ni-Based Superalloys Incorporating an Electrosynthesized Ceria Diffusion Barrier. *Mater. Chem. Phys.* 143, 416–424. doi:10.1016/j.matchemphys.2013.09.022

Goral, M., Ochal, K., Kubaszek, T., and Drajewicz, M. (2020). The Influence of Deposition Technique of Aluminide Coatings on Oxidation Resistance of Different Nickel Superalloys. *Mater. Today Proc.* 33, 1746–1751. doi:10.1016/j.matpr.2020.04.863

Goward, G. W., and Boone, D. H. (1971). Mechanisms of Formation of Diffusion Aluminide Coatings on Nickel-Base Superalloys. *Oxid. Mater.* 3, 475–495. doi:10.1007/bf00604047

Goward, G. W. (1970). Current Research on the Surface Protection of Superalloys for Gas Turbine Engines. *JOM* 22, 31–39. doi:10.1007/bf03355665

Huang, Y., Peng, X., and Chen, Q. (2019). TiO2 Nanoparticles-Assisted α-Al2O3 Direct Thermal Growth on Nickel Aluminide Intermetallics: Template Effect of the Oxide with the Hexagonal Oxygen Sublattice. *Corros. Sci.* 153, 109–117. doi:10.1016/j.corsci.2019.03.025

Huang, Y., and Peng, X. (2016). The Promoted Formation of an α-Al 2 O 3 Scale on a Nickel Aluminide with Surface Cr 2 O 3 Particles. *Corros. Sci.* 112, 226–232. doi:10.1016/j.corsci.2016.07.029

Khana, A., Huang, Y., Dong, Z., and Peng, X. (2019). Effect of Cr_2O_3 Nanoparticle Dispersions on Oxidation Kinetics and Phase Transformation of Thermally Grown Alumina on a Nickel Aluminide Coating – ScienceDirect. *Corros. Sci.* 150, 91–99.

Leng, W., Pillai, R., Naumenko, D., Galiullin, T., and Quadakkers, W. J. (2020). Effect of Substrate Alloy Composition on the Oxidation Behaviour and Degradation of Aluminide Coatings on Two Ni Base Superalloys. *Corros. Sci.* 167, 81–99. doi:10.1016/j.corsci.2020.108494

Liu, G., Li, M., Zhu, M., and Zhou, Y. (2007). Transient of Alumina Oxide Scale on β-NiAl Coated on M38G Alloy at 950°C. *Intermetallics* 15, 1285–1290. doi:10.1016/j.intermet.2007.03.010

Mollard, M., Rannou, B., Bouchaud, B., Balmain, J., Bonnet, G., and Pedraza, F. (2013). Comparative Degradation of Nickel Aluminized by Slurry and by Pack Cementation under Isothermal Conditions. *Corros. Sci.* 66, 118–124. doi:10.1016/j.corsci.2012.09.009

Montero, X., Galetz, M. C., and Schütze, M. (2013). Low-activity Aluminide Coatings for Superalloys Using a Slurry Process Free of Halide Activators and Chromates. *Surf. Coatings Technol.* 222, 9–14. doi:10.1016/j.surfcoat.2013.01.033

Nicholls, J. R. (2003). Advances in Coating Design for High-Performance Gas Turbines. *MRS Bull.* 28 (9), 659–670. doi:10.1557/mrs2003.194

Peng, X., Clarke, D. R., and Wang, F. (2003). Transient-alumina Transformations during the Oxidation of Magnetron-Sputtered CoCrAl Nanocrystalline Coatings. *Oxid. Metals* 60, 225–240. doi:10.1023/a:1026015101783

Pint, B. A., Treska, M., and Hobbs, L. W. (1997). The Effect of Various Oxide Dispersions on the Phase Composition and Morphology of Al2O3 Scales Grown on β-NiAl. *Oxid. Met.* 47, 1–20. doi:10.1007/bf01682369

Swadba, L., Nawrat, G., Mendala, B., and Goral, M. (2011). The Influence of Deposition Process on Structure of Platinum-Modified Aluminide Coatings O Ni-Base Superalloy. *Key Eng. Mat.* 465, 247–250.

Tolpygo, V. K., and Clarke, D. R. (2000). Microstructural Study of the Theta-Alpha Transformation in Alumina Scales Formed on Nickel-Aluminides. *Mater. A. T. High. Temp.* 17, 59–70. doi:10.1179/mht.2000.011

Veal, B. W., Paulikas, A. P., and Birtcher, R. C. (2006). Mechanisms and Control of Phase Transition in Thermally Grown Aluminas. *Appl. Phys. Lett.* 89, 505. doi:10.1063/1.2364124

Wang, X., Peng, X., Tan, X., and Wang, F. (2016). The Reactive Element Effect of Ceria Particle Dispersion on Alumina Growth: A Model Based on Microstructural Observations. *Sci. Rep.* 6, 29593, 1–10. doi:10.1038/srep29593

Wang, Y. D., and Zhou, Y. B. (2012). Cyclic-Oxidation of RexOy-Modified Aluminide Coating. *Amr* 557-559, 1721–1726. doi:10.4028/www.scientific.net/amr.557-559.1721

Warnes, B. M., and Punola, D. C. (1997). Clean Diffusion Coatings by Chemical Vapor Deposition. *Surf. Coatings Technol.* 94-95, 1–6. doi:10.1016/s0257-8972(97)00467-2

Xu, C., Peng, X., and Wang, F. (2010). Cyclic Oxidation of an Ultrafine-Grained and CeO2-Dispersed δ-Ni2Al3 Coating. *Corros. Sci.* 52, 740–747. doi:10.1016/j.corsci.2009.10.034

Yavorska, M., Sieniawski, J., Filip, R., and Gancarczyk, T. (2011). Microstructure Investigation of Aluminide Coatings after Platinum Modification Deposited by CVD Method on Inconel 713 LC Ni-Base Superalloy. *Amr* 409, 883–888. doi:10.4028/www.scientific.net/amr.409.883

Yin, Q. F., and Zhen, R. (2015). Effect of Y_2O_3 on Microstructure and Oxidation Resistance Behavior of Aluminide Coating on Ni-Based Superalloy. *Adv. Mat. Res.* 13, 603–607.

Conflict of Interest: The authors declare that the research was conducted in the absence of any commercial or financial relationships that could be construed as a potential conflict of interest.

Publisher's Note: All claims expressed in this article are solely those of the authors and do not necessarily represent those of their affiliated organizations, or those of the publisher, the editors, and the reviewers. Any product that may be evaluated in this article, or claim that may be made by its manufacturer, is not guaranteed or endorsed by the publisher.